



Research paper

Calix[8]arene-based Ni^(II) complexes for electrocatalytic CO₂ reduction

Carlos A. Reyes-Mata, Ivan Castillo*

Instituto de Química, Universidad Nacional Autónoma de México, Circuito Exterior, CU, Ciudad de México 04510, Mexico



ARTICLE INFO

Keywords:
Calixarene
Nickel
Electrochemistry
Carbon dioxide

ABSTRACT

The electrochemical behavior and catalytic activity for the electroreduction of CO₂ of complexes of Ni^(II) containing phenanthroline-based ligands, with or without a calixarene scaffold, were tested. The complexes were characterized by spectroscopic techniques, and their electrocatalytic properties determined by cyclic voltammetry. With water as proton source the complex [(1,5-(2,9-dimethyl-1,10-phenanthro)-*p*-*tert*-butylcalix[8]arene) NiCl₂] (1) presented a significant increase in current at $E = -2.36$ V (relative to Ag/AgCl reference electrode) when reduced under an atmosphere of CO₂, indicating that an electrocatalytic process occurs. Thus, calix[8]arenes that feature a phenanthrolyl moiety as bidentate *N*-ligands, and an intramolecular proton source in the phenolic –OH groups, afford Ni^(II) electrocatalysts for the reduction of CO₂.

1. Introduction

The great activity of nickel in catalytic systems has been studied extensively [1], such that at the beginning of the 20th century, Paul Sabatier referred to it as a “spirited horse”; this was partly due to the difficulty in controlling its reactivity, which affects the selectivity of a desired chemical transformation [2]. Careful design of ligand scaffolds has allowed the taming of nickel reactivity, with examples in polymerizations (e.g. ethylene) [3], Suzuki-Miyaura couplings [4], C–S bond formation [5], activation of unsaturated molecules [6], and CO₂ reduction. The latter represents a global challenge due to the deleterious effect of CO₂ as a greenhouse gas. The transition metals are good candidates to carry out this transformation due to the ease of access to various oxidation states, allowing the electron/proton transfer; one of the earth-abundant candidates is nickel [7]. This is particularly relevant since CO₂ reduction has been inspired by the reactivity of CO-dehydrogenase, which has a nickel center at its active site [8]. Nevertheless, reductive carboxylation with nitrogen-containing ligands has been widely studied using different organic substrates as alkynes [9], organic (pseudo)halides [10], and esters [11] to produce the corresponding carboxylic acids with CO₂. On the other hand, through electroreduction, specifically with nickel/nitrogen-based catalysts, carbon monoxide [12], formate [13], and oxalate [14] can be produced. Despite the number of nickel-based catalysts with nitrogen-containing motifs, supramolecular catalysts with this metal are scarce.

In this context, calix[8]arenes represent an ideal platform for the binding of metal ions within their large cavities, while functionalization afford the opportunity to introduce different donor groups [15]. We

have thus exploited a calix[8]arene-based copper catalyst in selective and efficient C–S cross-coupling reactions [16]. Calix[8]arene was thus functionalized with a phenanthroline motif to afford the ligand **C8Phen** (Fig. 1), with its Cu(I) complexes as efficient catalysts for C–S couplings that result in a variety of diaryl sulfides. The selectivity of the substrates was affected by the steric restriction provided by the calixarene cavity, leading to enhanced reactivity of bromoarenes relative to their iodoarene counterparts. Confined environments may thus result in different reactivity and selectivity from that observed at a metal center exposed to bulk solvent, allowing reaction pathways that favor molecular collisions within the cavity, while also enforcing size restrictions. Based on these results, we are interested in expanding the scope of these compounds towards CO₂ reduction. Herein, we report the results of the catalytic electroreduction studies of nickel complexes with **C8Phen**, and neocuproine (**Neo**) ligands for CO₂ reduction.

2. Experimental

2.1. Reagents and techniques

All reagents and solvents were obtained from commercial sources. Air-sensitive compounds were handled under an inert atmosphere using standard Schlenk techniques or a nitrogen-filled glovebox. The synthesis of *p*-*tert*-butylcalix[8]arene was carried out according to the literature procedure [16]. IR spectra were acquired with a Perkin Elmer 203-B FT-IR spectrophotometer in the range of 4000–400 cm⁻¹ as KBr pellets. ¹H NMR spectra were recorded with a JEOL Eclipse 300 spectrometer, and tetramethylsilane as internal standard. Positive-ion Fast

* Corresponding author.

E-mail address: joseivan@unam.mx (I. Castillo).

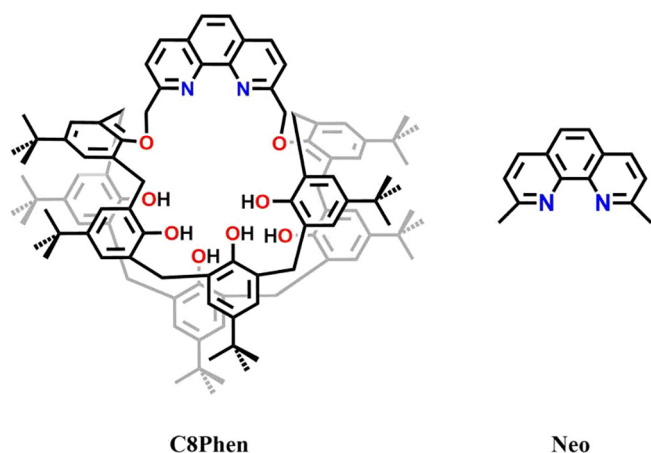


Fig. 1. Schematic representation of **C8Phen** and **Neo**.

Atom Bombardment mass spectra (FAB⁺) were measured on a JEOL JMS-SX-102A spectrometer, and direct analyses in real time mass spectra (DART) were acquired with a JEOL JMS-T100LC spectrometer. Combustion analyses were recorded with a Thermo Scientific Flash 2000. Melting points were determined with an Electrothermal Mel-Temp, without corrections.

Catalytic tests were carried out with standard Schlenk techniques, monitored by thin layer chromatography using silica gel GF-254 Merck, and revealed with short wave UV–vis light (254 nm). The products were purified by chromatography column using basic alumina 90 Macherey-Nagel as stationary phase and hexane as eluant.

2.2. Synthetic procedures

2.2.1. Synthesis of *p*-tert-butylcalix[8]arene

The *p*-tert-butylcalix[8]arene was synthesized according to the literature procedure [17], from *p*-tert-butylphenol (4.00 g, 0.026 mol), paraformaldehyde (3.60 g, 0.120 mol), and sodium hydroxide (355 mg, 0.008 mol) in xylene, by heating to reflux for 24 h under inert atmosphere. After cooling to room temperature, the solid formed was filtered and washed with cold xylene. The product was obtained as a white crystalline solid in 80% yield (3.40 g); m.p. > 250 °C (dec). ¹H NMR (CDCl₃, 300 MHz): δ 9.62 (s, 8H; OH), 7.17 (m, 16H; Ar), 4.36 (m, 8H; –CH₂–), 3.50 (m, 8H; –CH₂–), 1.25 (s, 72H; *t*-Bu).

2.2.2. Synthesis of 2,9-dimethyl-1,10-phenanthroline (NeoBr₂)

2,9-dimethyl-1,10-phenanthroline was synthesized from neocuproine (1.50 g, 0.007 mol) and three equivalents of recrystallized *N*-bromosuccinimide (4.00 g, 0.02 mol) in CH₃CN by refluxing for 18 h under inert atmosphere. After cooling to room temperature and evaporation under reduced pressure, the mixture was redissolved in diethylether and vacuum filtered. The solid was neutralized with a saturated solution of NaHCO₃. After, the solid was dissolved in THF and cooled to 0 °C, two equivalents of both HPO(OEt)₂ and *i*-Pr₂NEt were added, the mixture was warmed to room temperature, and stirred for 24 h for debromination. Then the solvent was evaporated under reduce pressure, and the product was purified by column chromatography using CH₂Cl₂ as eluant to obtain NeoBr₂ in 30% yield (800 mg); m.p. 110–115 °C (dec). ¹H NMR (CDCl₃, 300 MHz): δ 8.26 (d, *J* = 8.34 Hz, 2H, Ar), 7.92 (d, *J* = 8.33 Hz, 2H, Ar), 7.81 (s, 2H, Ar), 4.97 (s, 4H, CH₂Br). DART-MS *m/z* = 367 [NeoBr₂H]⁺.

2.2.3. Synthesis of 1,5-(2,9-dimethyl-1,10-phenanthro)-*p*-tert-butylcalix[8]arene (**C8Phen**)

The ligand **C8Phen** was obtained by adapting a literature method [18]. *p*-tert-butylcalix[8]arene (1.00 g, 0.77 mmol) and CsF (1.17 g, 7.70 mmol) were dried for two hours at 120 °C under vacuum. After

cooling to room temperature, THF was added and the mixture was heated to 50 °C overnight. After cooling to room temperature, NeoBr₂ (350 mg, 0.02 mmol) was added to the mixture and stirred for 36 h. The solvent was then evaporated under reduced pressure to afford a yellow solid that was dissolved in a CHCl₃/toluene 8:1 mixture, and after slow evaporation a crystalline solid was obtained. This solid was washed with 50 mL of HCl (0.1 M) and 30 mL of CH₂Cl₂ in order to remove cesium as CsCl. Finally, the product was washed with a saturated solution of NaHCO₃ for neutralization, affording **C8Phen** in 86% yield (800 mg); m.p. 245 °C (dec). IR (KBr) $\nu_{\max}/\text{cm}^{-1}$: 3230 (OH), 1594 (CN). ¹H NMR (C₂D₂Cl₄, 300 MHz): δ 9.52 (s, 6H, OH), 8.39 (d, *J* = 8.26 Hz, 2 H, Ar_{phen}), 7.89 (m, 2 H, Ar_{phen}), 7.24 (s, 2 H, Ar_{phen}), 7.10 (m, 16H, Ar_{calix}), 5.12 (s, 4 H, CH_{2phen}), 4.3 (m, *J* = 13 Hz, 8 H, CH_{2calix}), 3.54 (m, *J* = 13 Hz, 8 H, CH_{2calix}), 1.30 (m, 54H, *t*-Bu), 1.04 (m, 18H, *t*-Bu). FAB-MS *m/z* = 1502 [C8PhenH]⁺.

2.2.4. Synthesis of complexes

2.2.4.1. Synthesis of C8PhenNiCl₂ (1). The complex **C8PhenNiCl₂** was obtained from the reaction of **C8Phen** (50 mg, 0.033 mmol) and NiCl₂·6H₂O (7.80 mg, 0.033 mmol) in THF and stirring for 2 h at room temperature. Volatiles were evaporated and the solid was washed with diethylether to afford **C8PhenNiCl₂** as a pale yellow solid in 90% yield (48 mg); m.p. 270 °C (dec). Anal. Cald. for C₁₀₂H₁₂₀Cl₂N₂NiO₈·2CH₂Cl₂·H₂O; C: 68.65, H: 6.98, N: 1.54; Found C: 68.35, H: 6.77, N: 1.26. IR (KBr) $\nu_{\max}/\text{cm}^{-1}$: 3271 (OH), 1597 (CN). ¹H NMR (CDCl₃, 300 MHz): δ 9.7 (s, 6H, OH), 8.3 (s, 2 H, Ar_{phen}), 8.15 (s, 2 H, Ar_{phen}), 7.8 (s, 2 H, Ar_{phen}), 7.3 (m, 16H, Ar_{calix}), 5.2 (s, 4 H, CH_{2phen}), 4.45 (s, 8 H, CH_{2calix}), 3.5 (s, 8 H, CH_{2calix}), 1.3 (m, 72H, *t*-Bu). FAB-MS *m/z* = 1559 [C8PhenNi]⁺.

2.2.4.2. Synthesis of C8PhenNi(OAc)₂ (2). **C8PhenNi(OAc)₂** was obtained from the reaction of **C8Phen** (50 mg, 0.033 mmol) and Ni(OAc)₂·4H₂O (8.2 mg, 0.033 mmol) in THF and stirring for 2 h at room temperature. Volatiles were evaporated and the solid was washed with diethylether to afford **C8PhenNi(OAc)₂** as a yellow solid in 95% yield (53 mg); m.p. 290 °C (dec). Anal. Cald. for C₁₀₆H₁₂₆N₂NiO₁₂·CH₂Cl₂·H₂O; C: 72.13, H: 7.35, N: 1.57; Found C: 72.26, H: 7.19, N: 1.47. IR (KBr) $\nu_{\max}/\text{cm}^{-1}$: 3249 (OH), 1598 (CN), 1573 and 1479 (CH₃COO). ¹H NMR (CDCl₃, 300 MHz): δ 9.63 (s, 6H, OH), 8.24 (s, 2 H, Ar_{phen}), 7.88 (s, 2 H, Ar_{phen}), 7.18 (s, 16H, Ar_{calix}), 4.36 (m, 8 H, CH_{2calix}), 3.34 (m, 8 H, CH_{2calix}), 1.26 (m, 72H, *t*-Bu). FAB-MS *m/z* = 1559 [C8PhenNi]⁺.

2.2.4.3. Synthesis of NeoNiCl₂ (3). The complex **NeoNiCl₂** was synthesized from the reaction of neocuproine (50 mg, 0.24 mmol) and NiCl₂·6H₂O (57 mg, 0.24 mmol) in MeOH, and stirring for 2 h at room temperature. After evaporation of volatiles, the solid was washed with diethylether to afford **NeoNiCl₂** as a dark green solid in 95% yield (77 mg); m.p. > 350 °C (dec). Anal. Cald. for C₁₄H₁₂Cl₂N₂Ni·3H₂O; C: 42.91, H: 4.63, N: 7.15; Found C: 42.34, H: 4.02, N: 6.96. IR (KBr) $\nu_{\max}/\text{cm}^{-1}$: 3282 (H₂O), 1613–1504 (C–H ar). ¹H NMR (MeOD, 300 MHz): δ (ppm) = 68 (s, 2H, Ar_{phen}), 20 (s, 2H, Ar_{phen}), 18 (s, 2H, Ar_{phen}), –2 (s, 2H, CH₃). DART-MS *m/z* = 359 [NeoNiCl₂Na]⁺, 301 [NeoNiCl]⁺.

2.2.4.4. Synthesis of NeoNi(OAc)₂ (4). The complex **NeoNi(OAc)₂** was synthesized from the reaction of neocuproine (50 mg, 0.24 mmol) and Ni(OAc)₂·4H₂O (60 mg, 0.24 mmol) in MeOH, and stirring for 2 h at room temperature. Volatiles were evaporated under reduced pressure and the solid was washed with diethylether to obtain the complex **NeoNi(OAc)₂** as a light green solid in 98% yield (90 mg); m.p. > 350 °C (dec). Anal. Cald. for C₁₈H₁₈N₂NiO₄·H₂O; C: 53.64, H: 5.00, N: 6.95; Found C: 53.81, H: 4.71, N: 6.75. IR (KBr) $\nu_{\max}/\text{cm}^{-1}$: 3447 (H₂O), 1538 and 1449 (CH₃COO). ¹H NMR (MeOD, 300 MHz): δ (ppm) = 53 (s, 8H, Ar_{phen}, CH₃COO), 20 (s, 2H, Ar_{phen}), 17.5 (s, 2H, Ar_{phen}), –9.5 (s, 6H, CH₃). DART-MS *m/z* = 325 [NeoNiOAc]⁺, 209 [NeoH]⁺.

2.3. Cyclic voltammetry

Electrochemical characterization of the complexes and CO₂ electroreduction studies were carried out using a CH instruments 1200B potentiostat with a three electrodes cell equipped with a 3 mm diameter glassy carbon working electrode, platinum wire as counter electrode, and Ag⁺/Ag reference electrode with a tetrabutylammonium bromide (Bu₄NBr) solution. The supporting electrolyte used was tetrabutylammonium hexafluorophosphate (Bu₄NPF₆) 0.1 M in 5 mL THF or 5 mL CH₃CN:THF (95:5). The measured potentials at the working electrode are reported with respect to the ferrocenium/ferrocene (Fc⁺/Fc) couple, by adding ferrocene to the solutions at the end of each experiment. Dioxxygen was removed by bubbling with dinitrogen.

3. Results and discussion

3.1. Synthesis and characterization

The first step was the synthesis of *p*-*tert*-butylcalix[8]arene (**C8**) according to the methodology reported by Gutsche [17], which afforded **C8** as a white powder in good yield. The second step was to functionalize the neocuproine through a bromination reaction to obtain **NeoBr**₂; while the yield is moderate, characterization confirms its identity for subsequent steps. Finally, the ligand 1,5-(2,9-dimethyl-1,10-phenanthro)-*p*-*tert*-butylcalix[8]arene (**C8Phen**) was obtained from the initial reaction of **C8** and CsF as template for 12 h in THF, followed by addition of **NeoBr**₂ (Scheme 1). This results in the selective functionalization at the 1,5 positions of the calixarene. **C8Phen** was purified after eliminating cesium by washing with 0.1 N aqueous HCl by column chromatography with CH₂Cl₂ as eluent, obtaining the ligand in 80% yield.

The complexes of **C8Phen** with Ni^(II) salts were prepared by mixing the ligand with NiCl₂ and Ni(OAc)₂ in THF/MeOH and stirring for 2 h; we expected to determine if the different counterions may have an effect on the reactivity. The solids obtained as light yellow powders correspond to **C8PhenNiCl**₂ (**1**) and **C8PhenNi(OAc)**₂ (**2**) in good yields, 85% and 90%, respectively. In order to compare the influence of the calixarene motif, the corresponding complexes with neocuproine **NeoNiCl**₂ (**3**) and **NeoNi(OAc)**₂ (**4**) were also synthesized. The reactions were carried out in an analogous fashion, affording the complexes as green solids in 95% yield for the complex **3** and 98% yield for complex **4**.

Characterization of **C8Phen** and the nickel complexes by IR spectroscopy was undertaken, in order to determine the presence of acetate counterions in complexes **2** and **4**; the symmetric and asymmetric bands of those groups appear at 1479 and 1573 cm⁻¹ for **2**, and at 1449 and 1538 cm⁻¹ for **4** [19,20]. The separation between the symmetric and asymmetric stretching bands of the acetate groups provide information about their coordination mode. For both **2** and **4**, the difference of 94 and 89 cm⁻¹ indicates a bidentate coordination mode of the acetates

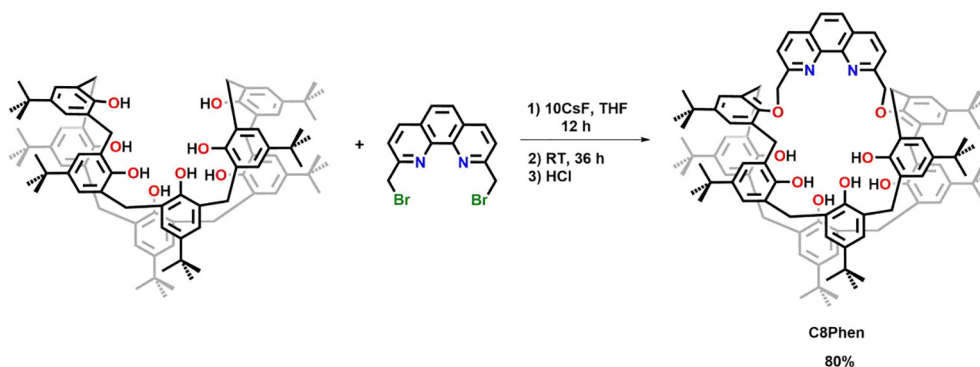
toward the Ni^(II) centers. The IR spectra of all compounds are presented in the ESI Figs. S1–S5.

Positive-ion Fast Atom Bombardment (FAB⁺) mass spectrometry analysis of **1** and **2** reveals in both cases a peak at *m/z* = 1559 that is assigned as [**C8PhenNi**]⁺, which corresponds to a Ni-reduced species that may form in the ionization chamber [21]. Complexes **3** and **4** were characterized by Direct Analysis in Real Time (DART) mass spectrometry. For **3**, the spectrum shows a peak at *m/z* = 359, assigned to [**NeoNiCl**Na]⁺, a peak at *m/z* = 301 assigned as [**NeoNiCl**]⁺, and at *m/z* = 209 corresponding to the protonated ligand [**NeoH**]⁺. Analysis of **4** reveals a peak at *m/z* = 325, which was assigned as [**NeoNiOAc**]⁺, as well as the peak corresponding to [**NeoH**]⁺ (ESI Figs. S6–S9).

¹H NMR spectroscopy of **C8Phen** was recorded in different solvents, with better definition of the signals in C₂D₂Cl₄ as shown in Fig. 2. This corresponds to the dicesium salt of doubly deprotonated **C8Phen**, namely [**C8Phen-2H**]²⁻Cs₂, since the cations appear to provide rigidity that allows assignment of the signals, as previously reported by our group in a variable-temperature study [18]. The protic H atoms are expected to be exchangeable, giving rise to a broad signal at 9.55 and a shoulder near the phenanthrolyl resonances at 8.45 ppm, consistent with the two signals expected based on symmetry considerations. This behavior was further probed by addition of 1 μL of D₂O to a solution of [**C8Phen-2H**]²⁻Cs₂, resulting in disappearance of the broad signals (ESI, Fig. S10).

The ¹H NMR spectra of the complexes were recorded initially in CDCl₃. The spectrum of **1** (Fig. S11) shows the signals of the methylene groups of the calixarene framework as two doublets between 3.50 and 4.50 ppm as an AX system; the phenanthroline-CH₂-O protons at 5.2 ppm, and the signal of the OH groups around 9.70 ppm. The signals of the aromatic protons appear between 8 and 8.50 ppm. Complex **2** show a similar spectrum, highlighting the signals of the AX system at 3.34–4.36 ppm and the signal for the OH group at 9.63 ppm (Fig. S12). The complexes are not amenable for characterization by ¹³C NMR spectroscopy, likely due to their flexible nature, and the presence of the Ni^(II) paramagnetic centers that result in broad and poorly resolved signals. Nonetheless, the broadening and paramagnetic shift is not as marked as in the neocuproine complexes, likely due to the distance of the phenolic moieties to the paramagnetic Ni^(II) ions.

In contrast, the ¹H NMR spectra of the neocuproine complexes (**3** and **4**) showed resonances between 70 and –10 ppm, distinctive of paramagnetic species. In the high field region between –2 and –10 ppm, the signals observed were assigned to the protons of the **Neo**-methyl groups. The assignment was carried out starting from the integration of the signals for the aromatic protons of **Neo** between 17 and 21 ppm, corresponding to 2H each. This allowed us to determine that the signal at high field corresponds to the six methyl group protons, while the signals at low field were assigned to the remaining aromatic protons (Figs. S13 and S14). In the case of **4**, the intense signal at 53 ppm integrates to 8H, and was thus assigned to the aromatic protons



Scheme 1. Synthesis of **C8Phen**.

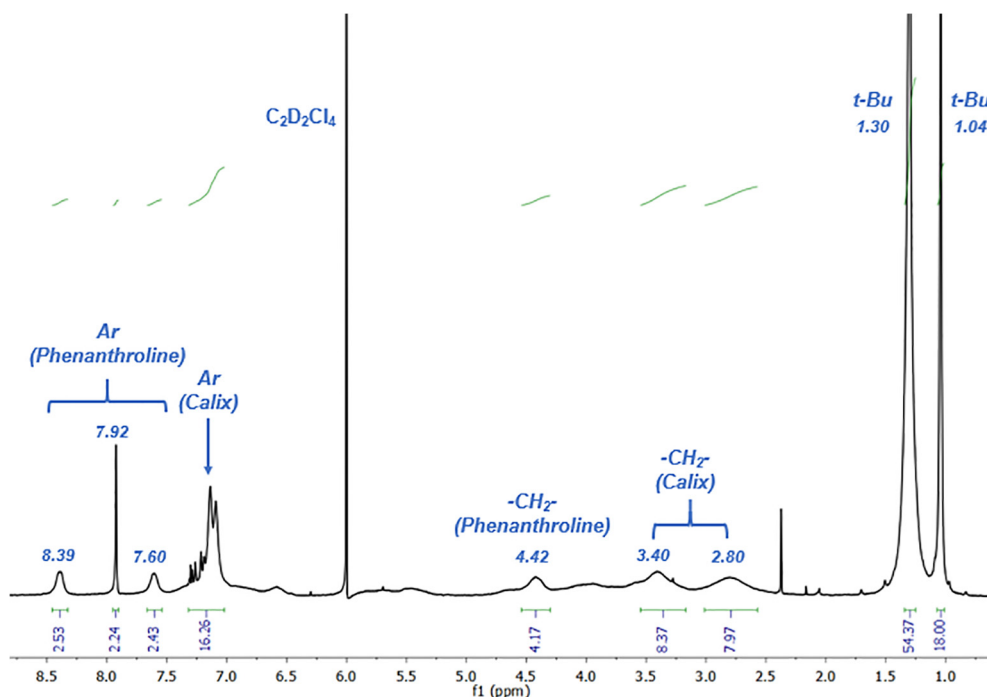


Fig. 2. ^1H NMR spectrum of $[\text{C8Phen-2H}]\text{Cs}_2$ in $\text{C}_2\text{D}_2\text{Cl}_4$ at 25°C (chemical shifts and assignments indicated).

of **Neo** (likely those in *para* position relative to the *N*-donors) overlapping with the signal corresponding to the acetate Me-groups.

3.2. Cyclic voltammetry

3.2.1. Electrocatalytic reduction activity

Initially, the behavior of the ligands **Neo** and **C8Phen** was interrogated by cyclic voltammetry (Fig. 3). It can be observed that **Neo** presents two irreversible reduction waves at -2.53 V and -2.76 V vs Fc^+/Fc . The first reduction can be attributed to the formation of the radical anion $\text{Neo}^{\cdot-}$, and the second reduction wave may be due to the generation of Neo^{2-} , as has been reported previously [22]. **C8Phen** shows a similar behavior, with two reduction processes at -2.51 and -2.77 V (Fig. 3). The reduction processes occur at very similar potentials, but they are better defined in the case of **C8Phen**.

The cyclic voltammogram of **1** presents two reduction waves: the first one at -2.01 V assigned to the $\text{Ni}^{\text{II}}/\text{Ni}^{\text{I}}$ redox couple, and at -2.36 V assigned to the $\text{Ni}^{\text{I}}/\text{Ni}^{\text{0}}$ reduction (Fig. 4a). Since CO_2 reduction is a Proton Coupled Electron Transfer (PCET) reaction, we tested different proton sources to analyze the behavior of **1** under an atmosphere of CO_2 , with water providing the best results. For this,

1 mM solutions of **1** in a $\text{CH}_3\text{CN}/\text{THF}$ (95:5) mixture were placed in a three-electrode cell, saturated with CO_2 by bubbling between each measurement. Increasing amounts of water were added to the cell to evaluate the influence of the proton source in the reaction. Fig. 4b shows that with 10% (v/v) of water added, the current measured reaches a minimum value. This happens under CO_2 atmosphere only, compared to when the proton source is present under N_2 atmosphere (Fig. S15), indicating that an electrocatalytic process occurs in the presence of CO_2 . With regard to complex **2**, its activity was significantly lower than that of **1**, and therefore we did not pursue its study further. Apparently, the presence of acetate counterions hinders the reactivity of the nickel centers in these systems.

In a preliminary assessment to establish the influence of the intramolecular protons contained in the ligand **C8Phen**, the electrocatalytic activity towards CO_2 reduction was carried out using Ni^{II} complexes with the methylated ligand **C8PhenMe** (Fig. 5). The first results show that the presence of the intramolecular protons is necessary for CO_2 reduction to occur, as it has been demonstrated previously in related proton-transfer processes [23].

For comparison purposes, characterization of **3** and **4** that feature the **Neo** ligand but lack the calixarene moiety was undertaken by cyclic

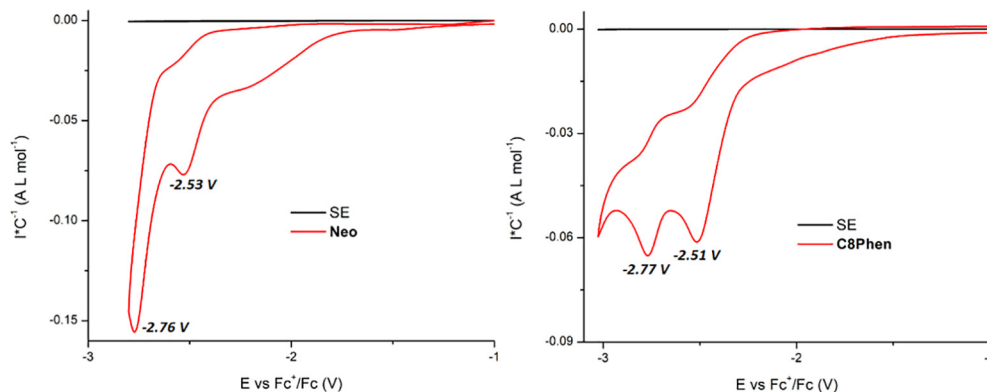


Fig. 3. Cyclic voltammograms of **Neo** (left), and **C8Phen** (right) under an atmosphere of N_2 . Conditions: 0.1 M Bu_4NPF_6 in $\text{CH}_3\text{CN}:\text{THF}$ (95:5) saturated with N_2 at 100 mV s^{-1} , glassy carbon working electrode, Ag/AgCl reference electrode. SE = Supporting Electrolyte.

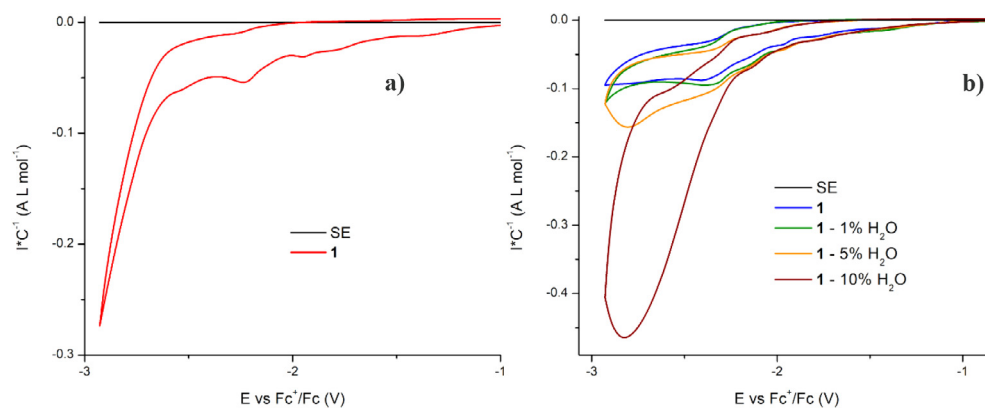


Fig. 4. Cyclic voltammograms of **1**: a) under an atmosphere of N_2 ; b) under an atmosphere of CO_2 and different percentages of water. Conditions: 0.1 M Bu_4NPF_6 in CH_3CN/THF at 100 mV s^{-1} .

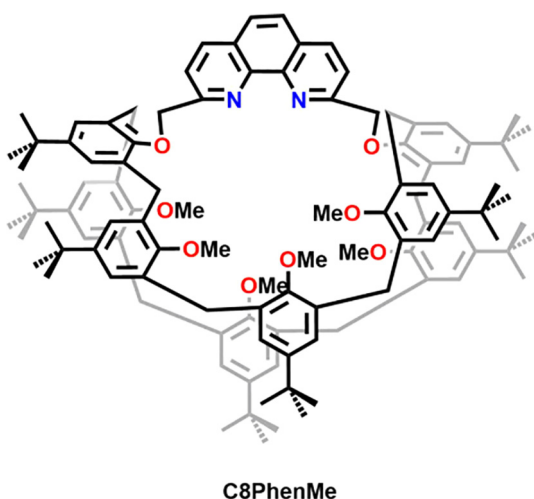


Fig. 5. Schematic representation of **C8PhenMe**.

voltammetry. Complex **3** showed three redox processes (Fig. 6a), the two first ones assigned as nickel-centered at $E_{1/2} = -1.20$ (Ni^{III}/Ni^{II}) with a difference between the anodic and cathodic peak potentials (ΔE_p) of 70 mV and $E_{1/2} = -1.53$ V ($Ni^{II}/Ni^{(0)}$) with $\Delta E_p = 80$ mV, and the one at more negative potential assigned to ligand-centered reduction observed at $E_{1/2} = -2.23$ V ($\Delta E_p = 70$ mV). **4** presents an irreversible reduction at -1.79 V, assigned to the Ni^{III}/Ni^{II} couple, and a S-shape wave reduction of the ligand at less negative potential relative to that of **3** ($E_{1/2} = -2.15$ V; $\Delta E_p = 135$ mV, Fig. 6b). When the atmosphere of dinitrogen is replaced by CO_2 , the S-shape waves of

the complexes disappear, likely due to an electron transfer process followed by a chemical step (ESI Fig. S16). This is consistent with irreversible binding of CO_2 to the reduced $Ni^{(0)}$ center, as described by Kubiak and coworkers [24]. Based on the current reached, the electrocatalytic activity of these complexes was not significantly better than that observed for the calixarene-based complex, e.g. for **3** vs **1** (compare ESI Fig. S17 with Fig. 4).

4. Conclusions

The electrocatalytic reduction of CO_2 is assisted by an external proton source, and the presence of an intramolecular source provided by **C8Phen** further facilitates this transformation, as determined based on comparisons with the **Neo**-based complexes. Characterization of the calixarene-based complex **1** by cyclic voltammetry showed two irreversible waves attributed to the two reduction processes centered on Ni. A better activity towards the reduction of CO_2 was observed when 10% (v/v) water is added, with the current reaching a minimum value relative to that determined under N_2 atmosphere. This indicates that an electrocatalytic process occurs under CO_2 atmosphere. Complexes **3** and **4** did not show significantly electrocatalytic activity, but their behavior in cyclic voltammetry allowed the electrochemical characterization of the nickel centers (Ni^{III}/Ni^{II}) and ($Ni^{II}/Ni^{(0)}$) in the case of **3**; for **4** only an irreversible reduction wave was observed. Under an atmosphere of CO_2 , the S-shape waves of the **Neo**-based complexes disappear, which can be attributed to an irreversible binding of the CO_2 to the nickel centers. The selectivity of the CO_2 reduction products by **1** is currently underway.

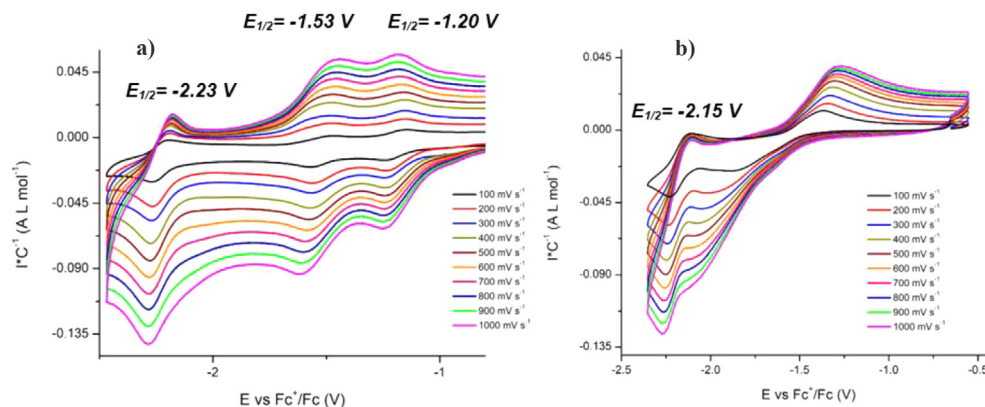


Fig. 6. Cyclic voltammograms of a) **3**, and b) **4**. Conditions: 0.1 M Bu_4NPF_6 in CH_3CN/THF (95:5) saturated with N_2 at 100 mV s^{-1} .

CRediT authorship contribution statement

Carlos A. Reyes-Mata: Investigation, Writing - original draft. **Ivan Castillo:** Supervision, Writing - review & editing.

Acknowledgements

The authors thank Luis Velasco for FAB-MS, Javier Pérez for DART-MS, Virginia Gómez-Vidales for EPR measurements, María de la Paz Orta for combustion analysis, Rocío Patiño for IR, Instituto de Química, UNAM, and Conacyt (Beca 308307) for financial support.

Appendix A. Supplementary data

Supplementary data to this article can be found online at <https://doi.org/10.1016/j.ica.2020.119607>.

References

- [1] (a) I.T. Trots, T. Zimmermann, F. Schüth, *Chem. Rev.* 114 (2014) 1761–1782; (b) G. Wilke, *Angew. Chem. Int. Ed.* 27 (1988) 185–206.
- [2] V.P. Ananikov, *ACS Catal.* 5 (2015) 1964–1971.
- [3] (a) M.A. Zuideveld, P. Wehrmann, C. Röhr, S. Mecking, *Angew. Chem. Int. Ed.* 43 (2004) 869–873; (b) L.A. Brown, W.C. Anderson, N.E. Mitchell, K.R. Gmernicki, *Polymers (Basel)* 10 (2018) 1–9.
- [4] C.A. Malapit, J.R. Bour, C.E. Brigham, M.S. Sanford, *Nature* 563 (2018) 100–104.
- [5] S.C. Lee, H.H. Liao, A. Chatupheeraphat, M. Rueping, *Chem. A Eur. J.* 24 (2018) 3608–3612.
- [6] (a) L. Cheng, M.M. Li, L.J. Xiao, J.H. Xie, Q.L. Zhou, *J. Am. Chem. Soc.* 140 (2018) 11627–11630; (b) Y. Zhang, X. Xu, S. Zhu, *Nat. Commun.* 10 (2019) 1–9.
- [7] J.W. Wang, W.J. Liu, D.C. Zhong, T.B. Lu, *Coord. Chem. Rev.* 378 (2019) 237–261.
- [8] (a) T. Fogeron, P. Retailleau, M. Gomez-Mingot, Y. Li, M. Fontecave, *Organometallics* 38 (2019) 1344–1350; (b) T. Fogeron, T.K. Todorova, J.P. Porcher, M. Gomez-Mingot, L.M. Chamoreau, C. Mellot-Draznieks, Y. Li, M. Fontecave, *ACS Catal.* 8 (2018) 2030–2038.
- [9] X. Wang, M. Nakajima, R. Martin, *J. Am. Chem. Soc.* 137 (2015) 8924–8927.
- [10] M. Börjesson, T. Moragas, D. Gallego, R. Martin, *ACS Catal.* 6 (2016) 6739–6749.
- [11] T. Moragas, J. Cornella, R. Martin, *J. Am. Chem. Soc.* 136 (2014) 17702–17705.
- [12] B. Fisher, R. Eisenberg, *J. Am. Chem. Soc.* 102 (1980) 7361–7363.
- [13] J.P. Collin, A. Jouaiti, J.P. Sauvage, *Inorg. Chem.* 27 (1988) 1986–1990.
- [14] M. Rudolph, S. Dautz, E.G. Jager, *J. Am. Chem. Soc.* 122 (2000) 10821–10830.
- [15] I. Abdellah, P. Kasongo, A. Labattut, R. Guillot, E. Schulz, C. Martini, V. Huc, *Dalton Trans.* 47 (2018) 13843–13848.
- [16] E. Guzmán-Percástegui, D.J. Hernández, I. Castillo, *Chem. Commun.* 52 (2016) 3111–3114.
- [17] C.E. Braun, C.D. Cook, J. Charles, Merritt, J.E. Rousseau, *Org. Synth.* 31 (1951) 77.
- [18] D.J. Hernández, H. Vázquez-Lima, P. Guadarrama, D. Martínez-Otero, I. Castillo, *Tetrahedron Lett.* 54 (2013) 4930–4933.
- [19] R. Baird, *Solubility and structure studies of nickel (II) acetate*, Masters Theses, Missouri, 1964.
- [20] K. Nakamoto, *Infrared and Raman Spectra of Inorganic and Coordination Compounds: Part B: Applications in Coordination, Organometallic, and Bioinorganic Chemistry*, Wiley, New Jersey, 2008.
- [21] J.N. Kyranos, P. Vouros, *Biol. Mass Spectrom.* 19 (1990) 628–634.
- [22] (a) H. Yi, A. Jutand, A. Lei, *Chem. Commun.* 51 (2015) 545–548; (b) A. Klein, A. Kaiser, B. Sarkar, M. Wanner, J. Fiedler, *Eur. J. Inorg. Chem.* (2007) 965–976; (c) D.G. Yakhvarov, A. Petr, V. Kataev, B. Büchner, S. Gómez-Ruiz, E. Hey-Hawkins, S.V. Kvashennikova, Y.S. Ganushevich, V.I. Morozov, O.G. Sinyashin, *J. Organomet. Chem.* 750 (2014) 59–64.
- [23] H. Diebler, F. Secco, M. Venturini, *J. Phys. Chem.* 88 (1984) 4229–4232.
- [24] A.L. Ostericher, T.M. Porter, M.H. Reineke, C.P. Kubiak, *Dalton Trans.* (2019) 15841–15848.